Enhancement of Photon Number Reflected by the Relativistic Flying Mirror

M. Kando,[1] A. S. Pirozhkov,[1] K. Kawase,[1] T. Zh. Esirkepov,[1] Y. Fukuda,[1] H. Kiriyama,[1] H. Okada,[1] I. Daito,[1] T. Kameshima,[1] Y. Hayashi,[1] H. Kotaki,[1] M. Mori,[1] J. K. Koga,[1] H. Daido,[1] A. Ya. Faenov,[1,*] T. Pikuz,[1,*] J. Ma,[1,†] L.-M. Chen,[1,†] E. N. Ragozin,[2] T. Kawachi,[1] Y. Kato,[1,‡] T. Tajima,[1,§] and S. V. Bulanov[1]

[1]*Advanced Photon Research Center, JAEA, 8-1-7 Umemidai, Kizugawa, Kyoto 619-0215, Japan*

[2]*P. N. Lebedev Physical Institute of the Russian Academy of Sciences, Leninsky prospekt 53, 119991 Moscow, Russia*

(Received 24 March 2009; revised manuscript received 30 August 2009; published 4 December 2009)

Laser light reflection by a relativistically moving electron density modulation (flying mirror) in a wake wave generated in a plasma by a high intensity laser pulse is investigated experimentally. A counterpropagating laser pulse is reflected and upshifted in frequency with a multiplication factor of 37–66, corresponding to the extreme ultraviolet wavelength. The demonstrated flying mirror reflectivity (from 3×10^{-6} to 2×10^{-5}, and from 1.3×10^{-4} to 0.6×10^{-3}, for the photon number and pulse energy, respectively) is close to the theoretical estimate for the parameters of the experiment.

DOI: 10.1103/PhysRevLett.103.235003 PACS numbers: 52.59.Ye, 52.35.Mw, 52.38.Ph

Short, coherent pulses in the extreme ultraviolet (XUV) to x-ray spectral range are important tools for applications in material science, structural biology of proteins, attosecond spectroscopy, etc. [1]. Several schemes have been proposed and studied intensively to generate ultrashort pulses, e.g., high harmonic generation in gases [2] or solids [3], free-electron lasers [4], plasma based x-ray lasers [5], and reflection from flying mirrors moving nearly at the speed of light [6,7]. These flying mirrors are dense electron shells formed in a breaking wake wave, excited by the intense, short pulse laser in underdense plasma. These shells partially reflect a counterpropagating laser pulse. The reflected pulse inherits properties of the incident electromagnetic wave, such as coherence, polarization, and pulse form. The reflected radiation wavelength is shortened as $\approx \lambda_s/(4\gamma_{\mathrm{ph}}^2)$ due to the double Doppler effect, where λ_s is the incident pulse wavelength, $\gamma_{\mathrm{ph}} = 1/[1-(v_{\mathrm{ph}}/c)^2]^{1/2}$ is the relativistic factor associated with the mirror, v_{ph} is its phase velocity, and c is the speed of light in vacuum. The relativistic mirror paradigm is fruitful for a wide range of problems in theoretical physics such as Unruh radiation [8], the Casimir effect [9], and nonlinear quantum electrodynamics [10]. In relativistic laser plasmas, the oscillating relativistic mirror concept plays a key role in the theory of high order harmonics generation [11], in ultrashort pulse generation [12], and in the high efficiency regimes of laser ion acceleration [13]. As noted in Ref. [6], focusing of the reflected light by the relativistic mirror into a focus spot, the size of which is determined by the shortened wavelength of the radiation, allows approaching the Schwinger limit where electron-positron pair creation from vacuum and effects of nonlinear vacuum permeability become significant [10].

The first demonstration of the laser light reflection and frequency upshift within the relativistic flying mirror scheme was reported in Refs. [7]. There remained several questions concerning how close the theoretical predictions on the flying mirror reflectivity could be approached under the conditions of the experiments. Another question is on the uniformity of the mirror surface because the reflecting dense electron shell is formed during the nonlinear wake wave breaking, which may cause mirror modulations and fragmentations preventing the high quality focusing of the reflected light. In this Letter, we have performed a series of experiments aimed at finding the answers to these questions. We used a high power laser system, which could provide a regime of more nonlinear interaction than employed in Ref. [7], in a configuration with the head-on collision of two laser pulses (Fig. 1). The head-on collision has advantages in providing better control for the overlapping in space and time of the two laser pulses and in achieving the conditions desired for the two pulse interaction mediated by the wake wave. For the mirror uniformity test we used a wide acceptance angle spectrograph.

The experiment was performed with the J-KAREN laser, a Ti:sapphire chirped pulse amplification (CPA) laser at JAEA [14]. In the experiment, the ~520 mJ laser beams were split into three beams by two pellicles after the compression. The first pellicle produced a probe beam and the transmitted beams were further split into driver (to excite the wakefield) and source (to be reflected) pulses. The typical energies of the driver and source beams were 400 and 42 mJ, respectively. The pulse-to-pulse energy stability was 11% in the standard deviation. Pulse durations of the driver and source beams were measured with a

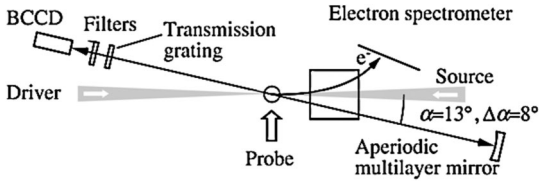

FIG. 1. A schematic of the experimental setup.

third-order transient grating frequency resolved optical gating [15] and were 27 and 34 fs at full width half maximum (FWHM), respectively. The contrast ratios at -100 and -500 ps were 10^{-7} and 10^{-6}, respectively.

The driver and source pulses were focused onto a helium gas-jet target by off-axis parabolic mirrors with the effective focal lengths of 475 and 775 mm, respectively. The laser pulses were set to collide head on. The laser light transmitted through the target returning to the laser system (''returning pulse'') was strongly attenuated by a spatial filter, Faraday isolators, and Pockels cells in the amplifier chain, and no instability nor damage were found during the experiment [16]. The attenuated laser spots in vacuum for the driver and source beams were 25×25 μm^2 and 43×66 μm^2, respectively, at $1/e^2$ intensity. The encircled energy ratios to the total energy in the spots were 72.3% and 73.4%, respectively. The estimated peak irradiances in vacuum were 6.5×10^{18} W/cm^2 and 1.2×10^{17} W/cm^2 for the driver and source, respectively. These irradiances correspond to the dimensionless amplitude [$a = eE/(mc\omega)$] of $a_d \approx 1.8$ for the driver and $a_s \approx 0.25$ for the source, where e and m are the electron charge and mass, E and ω are the electric field and angular frequency of the laser. The gas jet was provided by a pulsed solenoid valve and the nozzle had an orifice diameter of 1 mm with Mach number of 3.3. The density distribution was characterized by using a Mach-Zehnder interferometer. The FWHM length of the gas plume at the height of $Z = +1$ mm was 840 μm. The maximum plasma density was $(4.7 \pm 1.3) \times 10^{19}$ cm^{-3} at the absolute stagnation pressure of 2.1 MPa assuming the helium gas was fully ionized.

An electron spectrometer was installed 200 mm from the interaction point along the driver propagation axis. It was composed of a permanent magnet dipole with a size of 10×10 cm^2 and a field magnitude of 0.76 T, a phosphor screen (DRZ-High), and a gated image-intensified charge-coupled device (CCD). The detectable electron energy ranged from 10 to 160 MeV.

The reflected light was resolved by a normal incidence spectrograph (NIS), consisting of an aperiodic multilayer (Mo/Si) spherical mirror with a curvature radius of 500 mm and diameter of 50 mm, a transmission grating (5000 lines/mm) with a thickness of 0.5 μm and an area of 10×4 mm^2, free-standing Zr/Al multilayer optical blocking filters, and a back-illuminated CCD. The spherical mirror had a broadband uniform reflectivity of $\approx$10% from 12.5 to 30 nm [17] and the total detection wavelength range was 12.5–22 nm limited by the mirror and filters. The NIS covered the observation angles α from 9° to 17°. The imaging magnification was 2.37 and the CCD pixel size was 13.5 μm with a spatial resolution of 15 μm. Special effort was made to reduce noise on the CCD due to high energy electrons.

The two laser pulses (driver and source) were overlapped using shadowgrams taken with perpendicular probe beams, top-view images, far-field pattern images of the returning pulses, and spatially resolved spectra from the NIS (detailed description of these techniques will be presented elsewhere). Shadowgrams taken by varying the arrival time of the probe beams were used to align the vertical shift and colliding point (Fig. 2).

The observed signal in the NIS is shown in Fig. 3. In the raw image of the CCD shown in Fig. 3(a), zero order ($m = 0$) and $m = \pm 1$ and ± 2 diffraction orders are clearly seen. The similarity of the spectra of $m = 1$ and $m = -1$ shown in Fig. 3(b) confirms that the detected signal was resolved by the transmission grating, and was not from high energy photons due to bremsstrahlung by fast electrons. Because the supporting mesh of the transmission grating worked also as a perpendicular transmission grating of 250 lines/mm, lower resolution spectra in the perpendicular direction can be seen in the raw data. The spectrum had a broad bandwidth of 12.5–22 nm, which follows from the relationship between the reflected wavelength $\lambda_r(\alpha)$ and the observation angle α:

$$\lambda_r(\alpha) = \lambda_s(1 - \beta_{\mathrm{ph}} \cos\alpha)/(1 + \beta_{\mathrm{ph}}), \qquad (1)$$

where λ_s is the incident source wavelength and $\beta_{\mathrm{ph}} = v_{\mathrm{ph}}/c$. Substituting $a = 9°$–$17°$ from the experiment into Eq. (1), the expected spectrum is broad in contrast to the forward observation angle ($\alpha = 0°$) with small acceptance angle.

The photon flux measured with the NIS is $(1.85 \pm 0.05) \times 10^{11}$ photons/sr in 12.8–22.0 nm within the solid angle of $\Omega = 5.7$ msr. The errors are standard deviations due to CCD noise from hard x rays and do not include the systematic error. The helium gas surrounding the interaction region can absorb the radiation and decrease the observable number of photons. Therefore, we estimate that the flux at the interaction point is $(1.38 \pm 0.06) \times 10^{12}$ photons/sr.

From the observed spectrum, we determine the range of γ_{ph} in the actual shot. In order to obtain the same wavelength range of 12.8–22.0 nm in the observation angles of

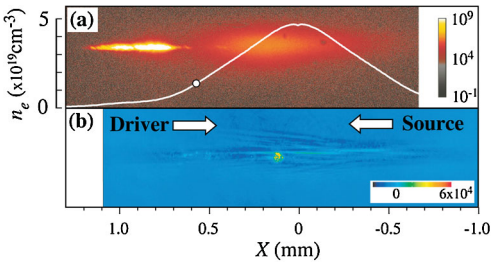

FIG. 2 (color). (a) Artificially superimposed top-view plasma image from two independent shots with driver (left) and source (right) only present. The line shows the plasma density distribution measured via interferometry. The open circle shows the colliding point in this particular shot ($x_0 = 580$ μm). (b) Shadowgram side view of two colliding pulses. The bright spot in the center is strong emission around the laser wavelength.

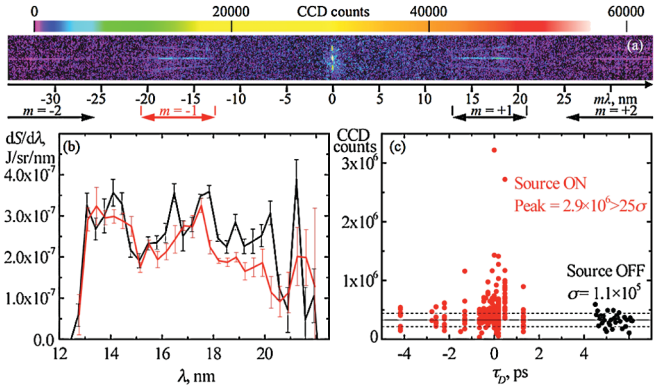

FIG. 3 (color). (a) Raw CCD image obtained with the normal incidence spectrograph. (b) Spectra in the diffraction order of $m = 1$ (black) and $m = -1$ (red). (c) CCD counts within the 1st diffraction order vs driver delay. The source off shots are shown for comparison, the delay is arbitrarily assigned.

$\alpha = 9°$–$17°$, the $\gamma_{\rm ph}$ should be in the range of 5–7 from Eq. (1). The factor $\gamma_{\rm ph}$ can also be estimated from the simplified relationship $\gamma_{\rm ph} \approx (n_{\rm cr}/n_e)^{1/2}$, where $n_{\rm cr}$ and n_e are the critical density and the plasma density, respectively. If we use the measured density, $(n_{\rm cr}/n_e)^{1/2} \approx 10$. Because this produces a rough estimate of $\gamma_{\rm ph}$, this estimation is in accordance with the measurements.

We also observed energetic electrons in the same shot as Figs. 3(a) and 3(b). The maximum electron energy in the nonlinear regime $E_{\rm max} \approx 2a_d^2\gamma_{\rm ph}^2 mc^2$ can be used to estimate $\gamma_{\rm ph}$ [18]. The maximum electron energy was >70 MeV, from which we obtain $\gamma_{\rm ph} \gtrsim 4.6$. The estimated $\gamma_{\rm ph}$ is also consistent with the previously obtained values.

Here, let us estimate the expected theoretical reflected photon number in the experiment. If we neglect the dependence of the reflectivity on the observation angle and only one flying mirror reflects photons, the reflectivity (in terms of photon number) of the flying mirror in a cusp structure for $\gamma_{\rm ph} \gg 1$ is $R_{\rm cusp} = 4^{-7/3}3^{-1/3}\Gamma^2(1/3) \times (\omega_{\rm pe}/\omega_s)^{8/3}\gamma^{-4/3}$, where $\Gamma(x)$ is the Euler gamma function, $\omega_{\rm pe}$ is the plasma frequency, and ω_s is the frequency of the source beam. The expected number of photons in a solid angle of Ω is $N_r = R_{\rm cusp}\, N_s\, (S_{\rm FM}/S_{\rm eff})$ [7], where N_s is the photon number in the source beam at the mirror, $S_{\rm FM} = r_{\rm FM}^2\Omega$ is the effective mirror area reflecting into a solid angle Ω, $r_{\rm FM}$ is the radius of the mirror, and $S_{\rm eff}$ is the effective area of the source beam. Here we assume a perfect overlap of the source pulse with the flying mirror. Then, we estimate the actual reflectivity using experimental parameters. As shown above, we can adopt $\gamma_{\rm ph} \approx 6$. Substituting $S_{\rm eff} = 800\ \mu{\rm m}^2$, $\omega_{\rm pe} = (4\pi e^2 n_e/m)^{1/2} = 2.3 \times 10^{14}/{\rm s}$, $r_{\rm FM} \approx \lambda_p = 4(2\gamma_{\rm ph})^{1/2}c/\omega_{\rm pe}$, $\Omega = 5.7$ msr we obtain $R_{\rm cusp} = 4 \times 10^{-5}$ and $N_r = 1.4 \times 10^{10}$ photons. The observed photon number $(1.05 \pm 0.03) \times 10^9$ photons, or $(7.9 \pm 0.3) \times 10^9$ photons accounting for the absorption in helium, is very close to the theoretical expectation.

The broadband and uniform spectrum observed in the experiment implies that the flying mirror in this solid angle was not a fragment but had a coherent structure.

The observed XUV source size was 16 μm at FWHM as seen in Fig. 3(a), which is approximately half of the source laser spot in vacuum. This value is most probably limited by the spatial resolution of the NIS.

When we changed the driver delay τ_D, the spatial position of the spot resolved by the NIS, x, changed. It is found to follow a linear function of the form $x = x_0 + c\tau_D/2$ when τ_D is adjusted so that the colliding point is upstream [upper half in Fig. 4(b)]. This is reasonable since the best reflecting point propagates together with the driver in this region. However, at time delays later than the best timing ($\tau_D \lesssim 0$), x remained the same (best colliding point) even if the driver delay was changed. This can be understood as follows. The group velocity of the wake wave is zero, and it remains broken at the same position, where the reflectivity is highest. This result excludes the possibility that the observed photons come from the reflection off the ionization front of the driver pulse [19].

The self-focusing facilitates the wave breaking under our experimental conditions. Although it can impair the wake wave regularity, the wake wave affords specular reflection, producing a coherent radiation. This is seen in our particle-in-cell (PIC) simulations performed with different laser pulse intensity and electron density as initial parameters, using the code REMP. In addition, the simulation illustrates the spatial localization of the wake wave excited by the laser pulse in inhomogeneous underdense plasma. A typical evolution of laser pulse and plasma is shown in Figs. 5(a)–5(c), where the Gaussian p-polarized driver laser pulse with $a_d = 2$, duration of 27 fs, and focal spot of 25 μm (FWHM) is focused in a fully ionized He gas at a distance of 240 μm from an *a posteriori* self-focusing position $x_{\rm sf}$ in a simulation with the box size of $320 \times 80\ \mu{\rm m}^2$, the mesh size of $1/20 \times 1/10\ \mu{\rm m}^2$, and

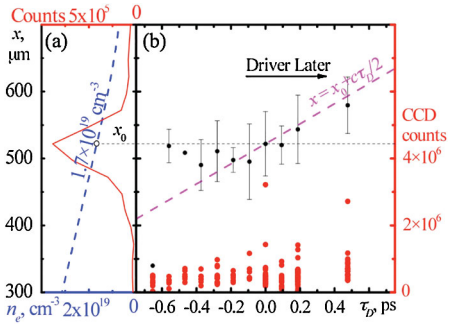

FIG. 4 (color). (a) CCD counts (solid line) and He atom density (dashed line) vs the distance to the gas-jet center x. The best collision point x_0 is marked with the open circle. (b) The signal spatial position vs the driver delay τ_D.

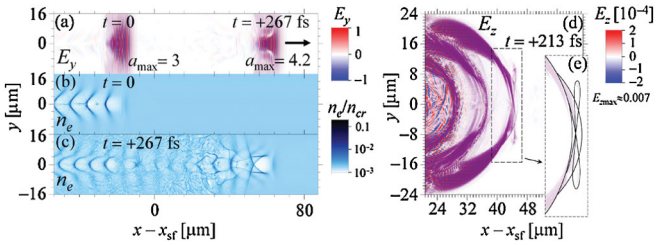

FIG. 5 (color). The laser pulse (a) self-focusing and the electron density (b),(c) evolution seen in the 2D PIC simulation. The self-focusing position x_{sf} corresponds to the collision point in Fig. 2. (d) The radiation reflected from the wake wave revealing an instantaneous pattern of the breaking wake wave (e).

the number of quasiparticles of 3.2×10^7. A regular wake wave appears in the region before the self-focusing position, Figs. 5(b) and 5(c), where it breaks providing optimal conditions for the source pulse reflection, in agreement with the result in Fig. 4. Figure 5(d) shows the reflection of the source pulse with $a_s = 0.15$, duration of 32 fs, and focal spot of 25 μm (FWHM), colliding with the driver at $x = x_{sf} + 20$ μm in an additional simulation performed using a moving window with the size of 120×100 μm^2, a finer mesh of $1/128 \times 1/32$ μm^2 and a higher number of quasiparticles of 3.9×10^9. In order to distinguish between the driver and reflected fields, the source pulse is set to be s polarized. Electron shells in several wake wave periods afford the specular reflection, in agreement with [20]. The reflected radiation is so coherent that it reveals an instantaneous pattern of the breaking wake wave, Fig. 5(e) (see Fig. 1 in Ref. [21]).

In conclusion, we have conducted a laser light reflection experiment from a breaking wake wave excited by an intense, short pulse laser in a head-on collision setup. The reflected photon number (energy) was 10^9–10^{10} photons (12–55 nJ) in the wavelength range from 12.8 to 22.0 nm within the detection angle of 5.7 msr. This corresponds to a 4000–50000 times increase compared to Ref. [7]. If we take into account the absorption of XUV light in the gas, the reflected photon number is close to the theoretical estimate with one mirror. The demonstrated flying mirror reflectivity is from 3×10^{-6} to 2×10^{-5}, and from 1.3×10^{-4} to 0.6×10^{-3}, for the photon number and pulse energy, respectively.

The source size of the reflected light was 16 μm FWHM (resolution limited), which was smaller than the incident source spot size. Recalling that the pulse duration of the reflected pulse scales as $\tau_r = \tau_s/(4\gamma_{ph}^2)$, the estimated peak brightness is $\sim 10^{22}$ photons/(mm^2 mrad^2 s) in 0.1% bandwidth. This is a lower-bound estimate, because the flying mirror focuses the reflected radiation to a much smaller spot than the spatial resolution. Since we have demonstrated high efficiency of relativistic flying mirrors, this allows one to design a future x-ray source based on this concept. Using a source laser energy of 1 J at $\gamma_{ph} = 10$ gives a mJ, attosecond pulse in the water-window wavelength region, which is suitable for live-cell imaging. The demonstrated high reflectivity is a milestone in realizing not only a novel x-ray source (attosecond, mJ, coherent) but also in accessing light intensification [6] towards the Schwinger field.

We thank T. Shimomura, Y. Nakai, M. Tanoue, A. Akutsu, T. Motomura, H. Sasao, D. Wakai, H. Matsuura, S. Kondo, and S. Kanazawa, for the laser operation, T. Homma for technical support, and M. Nishikino for providing the transmission grating. This work was supported by KAKENHI (20244065 and 19740252).

*Also at Joint Institute for High Temperature of the Russian Academy of Science, Moscow, Russia.
†Present address: Institute of Physics, Chinese Academy of Sciences, Beijing, China.
‡Present address: The Graduate School for the Creation of New Photonics Industries, Japan.
§Also at Ludwig-Maximilians-University, Germany.

[1] F. Krausz and M. Ivanov, Rev. Mod. Phys. **81**, 163 (2009), and references therein.
[2] P. B. Corkum and F. Krausz, Nature Phys. **3**, 381 (2007).
[3] B. Dromey *et al.*, Nature Phys. **5**, 146 (2009).
[4] G. Lambert *et al.*, Nature Phys. **4**, 296 (2008).
[5] H. Daido, Rep. Prog. Phys. **65**, 1513 (2002).
[6] S. V. Bulanov *et al.*, Phys. Rev. Lett. **91**, 085001 (2003).
[7] M. Kando *et al.*, Phys. Rev. Lett. **99**, 135001 (2007); A. S. Pirozhkov *et al.*, Phys. Plasmas **14**, 123106 (2007).
[8] L. Crispino *et al.*, Rev. Mod. Phys. **80**, 787 (2008).
[9] M. Bordag *et al.*, Phys. Rep. **353**, 1 (2001).
[10] G. Mourou *et al.*, Rev. Mod. Phys. **78**, 309 (2006); M. Marklund and P. Shukla, *ibid.* **78**, 591 (2006); Y. I. Salamin *et al.*, Phys. Rep. **427**, 41 (2006).
[11] S. V. Bulanov *et al.*, Phys. Plasmas **1**, 745 (1994); R. Lichters *et al.*, *ibid.* **3**, 3425 (1996); A. S. Pirozhkov *et al.*, *ibid.* **13**, 013107 (2006); C. Thaury *et al.*, Nature Phys. **3**, 424 (2007); A. Tarasevitch *et al.*, Phys. Rev. Lett. **98**, 103902 (2007).
[12] N. M. Naumova *et al.*, Phys. Rev. Lett. **92**, 063902 (2004): S. S. Bulanov *et al.*, Phys. Rev. E **73**, 036408 (2006); V. V. Kulagin *et al.*, Phys. Plasmas **14**, 113101 (2007); N. N. Rosanov, JETP Lett. **88**, 501 (2008); D. Habs *et al.*, Appl. Phys. B **93**, 349 (2008).
[13] T. Zh. Esirkepov *et al.*, Phys. Rev. Lett. **92**, 175003 (2004); F. Pegoraro and S. V. Bulanov, *ibid.* **99**, 065002 (2007).
[14] H. Kiriyama *et al.*, Opt. Commun. **282**, 625 (2009).
[15] A. S. Pirozhkov *et al.*, Advanced Solid-State Photonics, CD-ROM (OSA, Washington, DC, 2008), MC8.
[16] M. Kando *et al.*, Eur. Phys. J. D **55**, 465 (2009).
[17] I. L. Beigman *et al.*, JETP Lett. **74**, 149 (2001).
[18] E. Esarey and M. Pilloff, Phys. Plasmas **2**, 1432 (1995).
[19] M. Lampe, E. Ott, and J. H. Walker, Phys. Fluids **21**, 42 (1978); W. B. Mori, Phys. Rev. A **44**, 5118 (1991).
[20] A. V. Panchenko *et al.*, Phys. Rev. E **78**, 056402 (2008).
[21] S. V. Bulanov *et al.*, Phys. Rev. Lett. **78**, 4205 (1997).